Generalized Nuclear-Electronic Orbital Multistate Density Functional Theory for Multiple Proton Transfer Processes

Joseph A. Dickinson, Qi Yu, and Sharon Hammes-Schiffer*

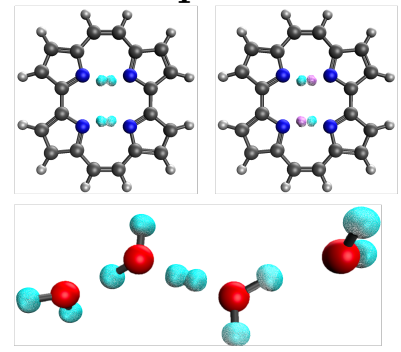
Department of Chemistry, Yale University, New Haven, Connecticut, 06520, USA

E-mail: sharon.hammes-schiffer@yale.edu

Abstract

Proton transfer and hydrogen tunneling play a pivotal role in many chemical and biological processes. The nuclear-electronic orbital multistate density functional theory (NEO-MSDFT) approach was developed to describe hydrogen tunneling systems within the multicomponent NEO framework, where the transferring proton is quantized and treated with molecular orbital techniques on the same level as the electrons. Herein, the NEO-MSDFT framework is generalized to an arbitrary number of quantum protons to allow applications to systems involving the transfer and tunneling of multiple protons. The generalized NEO-MSDFT approach is shown to produce delocalized, bilobal proton densities and accurate tunneling splittings for fixed geometries of the formic acid dimer and asymmetric substituted variants as well as the porphycene molecule. Investigation of a protonated water chain highlights the applicability of this approach to proton relay systems. This work provides the foundation for nuclear-electronic quantum dynamics simulations of a wide range of multiple proton transfer processes.





Hydrogen tunneling underlies many processes of chemical and biological interest. ^{1–3} Numerous methods have been developed to describe hydrogen tunneling systems, such as path integral approaches ^{3–6} and the multiconfigurational time-dependent Hartree method. ^{7–9} In contrast to these methods, the nuclear-electronic orbital (NEO) method accounts for nuclear quantum effects and non-Born-Oppenheimer effects directly within quantum chemistry calculations by quantizing certain nuclei, typically protons, and treating them with molecular orbital techniques at the same level as the electrons. ^{10,11} Nuclear delocalization, anharmonicity, zero-point energy, and nuclear tunneling are inherently included in NEO calculations, and excited vibronic states can be computed in a straightforward manner. The NEO method is therefore a natural framework with which to describe hydrogen tunneling phenomena.

Many methods based on both wavefunction theory ¹⁰⁻¹³ and density functional theory (DFT) ¹⁴⁻¹⁷ have been developed within the NEO framework. The NEO-DFT method in particular has been shown to be successful in describing hydrogen transfer phenomena. ¹⁸⁻²⁰ The success of NEO-DFT can be attributed to its effective balance between computational cost and accuracy, driven by its inclusion of electron-proton correlation through recently developed electron-proton correlation (epc) functionals. ^{15,16,21} However, a challenge for NEO-DFT is the description of hydrogen tunneling systems, where the hydrogen vibrational wavefunction delocalizes over the two wells of a double-well potential energy surface. ^{9,22,23} In NEO-DFT calculations, the protonic density tends to localize in one well of the double-well potential instead of delocalizing over both wells. ^{11,24,25} This localization is mainly due to the lack of static electron-proton correlation when the noninteracting reference system is described by a single product of an electronic and protonic determinant, as well as insufficient electron-proton dynamical correlation.

To address this challenge, the NEO multistate DFT (NEO-MSDFT) method was developed for describing hydrogen transfer and hydrogen tunneling systems within the NEO framework. Motivated by the conventional electronic MSDFT method, The NEO-MSDFT method linearly combines localized NEO-DFT states in a nonorthogonal configuration interaction scheme 1,32 in order to capture the bilobal, delocalized vibronic states needed to describe

hydrogen tunneling. The NEO-MSDFT method has been shown to produce accurate hydrogen tunneling splittings and proton densities for fixed molecular geometries involving one quantum proton. ²⁶ Analytical gradients of the NEO-MSDFT energies were also derived for the one-proton case, enabling geometry optimizations and minimum energy path calculations on NEO-MSDFT vibronic surfaces. ³³ The NEO-MSDFT method has also been combined with nonadiabatic dynamics methods such as Ehrenfest and surface hopping to describe the tunneling dynamics of the intramolecular proton transfer reaction in malonaldehyde. ³⁴

Herein, we present the generalized NEO-MSDFT approach to enable the simulation of more complex systems involving the transfer and tunneling of multiple quantum protons, such as proton relays, ^{35,36} water chains, ^{37–39} and hydrogen-bonding networks. ⁴⁰ After presenting the theory underlying this approach, we demonstrate its ability to predict accurate tunneling splittings and proton densities for the formic acid dimer ^{41–45} and substituted variants, porphycene, ⁵ and a protonated water chain. In addition to predicting hydrogen tunneling splittings, the NEO-MSDFT approach also offers a strategy for smoothly transitioning from one localized NEO-DFT solution to another during NEO quantum dynamics simulations, ³⁴ circumventing problems with local minima in orbital space while also allowing the proton to delocalize during proton transfer processes. ²⁰ Thus, this work provides the foundation for future nuclear-electronic quantum dynamics studies of systems in which multiple protons are transferring and, in some cases, tunneling.

Consider a system with N transferring protons, where each proton is moving in a double-well potential in the conventional Born-Oppenheimer picture. Quantizing each transferring proton within the NEO framework leads to 2^N diabatic NEO-DFT states. Each diabatic state has the protonic density of each transferring proton localized in one of the two wells of its corresponding double-well potential. For completeness, our derivation includes all possible combinations of each transferring proton localized near either its donor or acceptor, but in practice, higher-energy states can be excluded. The set of all diabatic NEO-DFT states is $\{|\tilde{\Psi}_0\rangle, |\tilde{\Psi}_1\rangle, \dots |\tilde{\Psi}_n\rangle\}$, where $n = 2^N - 1$. Each diabatic state is the product of a Kohn-Sham electronic and protonic determinant, with each determinant composed of electronic or protonic orbitals. For simplicity,

we assume closed-shell electronic and high-spin protonic configurations, but the extension to open-shell electronic configurations is straightforward.

The adiabatic NEO-MSDFT states $\{|\Psi_0\rangle, |\Psi_1\rangle, \dots |\Psi_n\rangle\}$ are linear combinations of all diabatic NEO-DFT states:

$$|\Psi_{0}\rangle = D_{0}^{0}|\tilde{\Psi}_{0}\rangle + D_{1}^{0}|\tilde{\Psi}_{1}\rangle + \dots + D_{n}^{0}|\tilde{\Psi}_{n}\rangle$$

$$|\Psi_{1}\rangle = D_{0}^{1}|\tilde{\Psi}_{0}\rangle + D_{1}^{1}|\tilde{\Psi}_{1}\rangle + \dots + D_{n}^{1}|\tilde{\Psi}_{n}\rangle$$

$$\vdots \qquad \vdots \qquad \vdots$$

$$|\Psi_{n}\rangle = D_{0}^{n}|\tilde{\Psi}_{0}\rangle + D_{1}^{n}|\tilde{\Psi}_{1}\rangle + \dots + D_{n}^{n}|\tilde{\Psi}_{n}\rangle$$

$$(1)$$

The coefficients in Eq. (1) are determined by solving the $2^N \times 2^N$ matrix eigenvalue problem

$$HD = SDE. (2)$$

The overlap matrix S contains the overlap between pairs of localized diabatic states

$$\mathbf{S} = \begin{bmatrix} S_{00} & S_{01} & \cdots & S_{0n} \\ S_{10} & S_{11} & \cdots & S_{1n} \\ \vdots & \vdots & \ddots & \vdots \\ S_{n0} & S_{n1} & \cdots & S_{nn} \end{bmatrix} = \begin{bmatrix} 1 & \langle \tilde{\Psi}_0 | \tilde{\Psi}_1 \rangle & \cdots & \langle \tilde{\Psi}_0 | \tilde{\Psi}_n \rangle \\ \langle \tilde{\Psi}_1 | \tilde{\Psi}_0 \rangle & 1 & \cdots & \langle \tilde{\Psi}_1 | \tilde{\Psi}_n \rangle \\ \vdots & \vdots & \ddots & \vdots \\ \langle \tilde{\Psi}_n | \tilde{\Psi}_0 \rangle & \langle \tilde{\Psi}_n | \tilde{\Psi}_1 \rangle & \cdots & 1 \end{bmatrix}$$
(3)

The off-diagonal elements of the overlap matrix S_{ij} for $i, j \in \{0, 1, ..., n\}$ are given by

$$S_{ij} = S_{ji} = \langle \tilde{\Psi}_i | \tilde{\Psi}_j \rangle = \left(\det \left(\mathbf{A}_{ij}^{\mathrm{e}} \right) \right)^2 \times \det \left(\mathbf{A}_{ij}^{\mathrm{p}} \right)$$
(4)

where the $\mathbf{A}_{ij}^{\mathrm{e}}$ and $\mathbf{A}_{ij}^{\mathrm{p}}$ matrices are given by

$$\mathbf{A}_{ij}^{e} = (\mathbf{C}_{i,o}^{e})^{\mathrm{T}} \mathbf{S}^{e} (\mathbf{C}_{j,o}^{e})$$

$$\mathbf{A}_{ij}^{p} = (\mathbf{C}_{i,o}^{p})^{\mathrm{T}} \mathbf{S}^{p} (\mathbf{C}_{j,o}^{p}).$$
(5)

The $C_{i,o}^e$ ($C_{i,o}^p$) and $C_{j,o}^e$ ($C_{j,o}^p$) matrices of Eq. (5) are the occupied blocks of the coefficient matrices of the electronic (protonic) parts of diabatic NEO-DFT states $|\tilde{\Psi}_i\rangle$ and $|\tilde{\Psi}_j\rangle$, respectively, and the S^e (S^p) matrices are the overlap matrices of the electronic (protonic) basis functions. Note that the electronic determinant in Eq. (4) is squared in the closed-shell treatment of electrons.

The effective Hamiltonian \mathbf{H} is given by

$$\mathbf{H} = \begin{bmatrix} H_{00} & H_{01} & \cdots & H_{0n} \\ H_{10} & H_{11} & \cdots & H_{1n} \\ \vdots & \vdots & \ddots & \vdots \\ H_{n0} & H_{n1} & \cdots & H_{nn} \end{bmatrix}$$
(6)

The diagonal matrix elements H_{ii} for $i \in \{0, 1, ..., n\}$ are given by $H_{ii} = E_i^{\text{NEO-DFT}} [\rho_i^{\text{e}}, \rho_i^{\text{p}}]$, which is the NEO-DFT energy of diabatic state $|\tilde{\Psi}_i\rangle$. Note that $E_i^{\text{NEO-DFT}} [\rho_i^{\text{e}}, \rho_i^{\text{p}}]$ is a functional of the electronic and protonic densities, ρ_i^{e} and ρ_i^{p} , of that diabatic state.

The off-diagonal matrix elements H_{ij} for $i, j \in \{0, 1, ..., n\}$ can be approximated in a manner analogous to MSDFT in conventional electronic structure ^{28,29,46} and NEO-MSDFT with a single transferring proton: ²⁶

$$H_{ij} = H_{ji} = \langle \tilde{\Psi}_{i} | \hat{H}_{NEO} | \tilde{\Psi}_{j} \rangle + \frac{1}{2} S_{ij} (E_{i}^{corr} + E_{j}^{corr})$$

$$= S_{ij} \Big(E_{nuc} + \text{Tr} \Big[\mathbf{P}_{ij}^{e} \mathbf{h}^{e} \Big] + \text{Tr} \Big[\mathbf{P}_{ij}^{p} \mathbf{h}^{p} \Big]$$

$$+ \frac{1}{2} \text{Tr} \Big[\mathbf{P}_{ij}^{e} \mathbf{J}^{ee} \mathbf{P}_{ij}^{e} \Big] + \frac{1}{2} \text{Tr} \Big[\mathbf{P}_{ij}^{p} \mathbf{J}^{pp} \mathbf{P}_{ij}^{p} \Big]$$

$$- \text{Tr} \Big[\mathbf{P}_{ij}^{e} \mathbf{J}^{ep} \mathbf{P}_{ij}^{p} \Big] - \frac{1}{4} \text{Tr} \Big[\mathbf{P}_{ij}^{e} \mathbf{K}^{ee} \mathbf{P}_{ij}^{e} \Big]$$

$$- \frac{1}{2} \text{Tr} \Big[\mathbf{P}_{ij}^{p} \mathbf{K}^{pp} \mathbf{P}_{ij}^{p} \Big] \Big) + \frac{1}{2} S_{ij} (E_{i}^{corr} + E_{j}^{corr}).$$

$$(7)$$

In Eq. (7), $\langle \tilde{\Psi}_i | \hat{H}_{\text{NEO}} | \tilde{\Psi}_j \rangle$ is the energy computed with the NEO Hamiltonian \hat{H}_{NEO} at the NEO Hartree-Fock (NEO-HF) level with the NEO Kohn-Sham determinants. Note that \hat{H}_{NEO} includes the kinetic energies of the electrons and quantum nuclei, as well as all the Coulomb

interactions between pairs of electrons, quantum nuclei, and classical nuclei. The correlation energies $E_i^{\rm corr}$ and $E_j^{\rm corr}$ are defined as the difference between the NEO-DFT and NEO-HF energies for states $|\tilde{\Psi}_i\rangle$ and $|\tilde{\Psi}_j\rangle$, respectively:

$$E_{i}^{\text{corr}} = E_{i}^{\text{NEO-DFT}} \left[\rho_{i}^{\text{e}}, \rho_{i}^{\text{p}} \right] - E_{i}^{\text{NEO-HF}} \left[\rho_{i}^{\text{e}}, \rho_{i}^{\text{p}} \right]$$

$$E_{j}^{\text{corr}} = E_{j}^{\text{NEO-DFT}} \left[\rho_{j}^{\text{e}}, \rho_{j}^{\text{p}} \right] - E_{j}^{\text{NEO-HF}} \left[\rho_{j}^{\text{e}}, \rho_{j}^{\text{p}} \right]$$
(8)

In Eq. (7), \mathbf{h} , \mathbf{J} , and \mathbf{K} represent the core Hamiltonian, Coulomb, and exchange terms, respectively, for electrons (e) and protons (p). E_{nuc} is the classical nuclear repulsion energy, and $\mathbf{P}_{ij}^{\text{e}}$ and $\mathbf{P}_{ij}^{\text{p}}$ are the transition density matrices between states $|\tilde{\Psi}_i\rangle$ and $|\tilde{\Psi}_j\rangle$ given by

$$\mathbf{P}_{ij}^{e} = 2\mathbf{C}_{i,o}^{e} \left[(\mathbf{A}_{ij}^{e})^{\mathrm{T}} \right]^{-1} (\mathbf{C}_{j,o}^{e})^{\mathrm{T}}$$

$$\mathbf{P}_{ij}^{p} = \mathbf{C}_{i,o}^{p} \left[(\mathbf{A}_{ij}^{p})^{\mathrm{T}} \right]^{-1} (\mathbf{C}_{j,o}^{p})^{\mathrm{T}}$$
(9)

The factor of two in the electronic transition density matrix arises in the case of a closed-shell treatment of electrons.

As in our previous work, 26,33,34 we account for the limitations of the epc functionals and the resulting inaccuracies of the overlap between two localized NEO-DFT states $\langle \tilde{\Psi}_i | \tilde{\Psi}_j \rangle$, as well as the approximate form of the off-diagonal Hamiltonian matrix elements, by applying a simple correction function to the off-diagonal elements of the **S** matrix:

$$S'_{ij} = \alpha (S_{ij})^{\beta}. \tag{10}$$

In most cases, the corrected overlap is greater than the uncorrected overlap, thus accounting for the slight proton density over-localization observed with the epc functionals. The working equations of the generalized NEO-MSDFT procedure with this corrected overlap are the same as those given above, except all instances of S_{ij} are replaced with S'_{ij} according to Eq. (10). For the epc17-2 electron-proton correlation functional, the α and β parameters were determined to be $\alpha = 0.0604$ and $\beta = 0.492$ based on fitting to the tunneling splittings for the FHF⁻ molecule at

different F-F distances.²⁶ This overlap correction procedure with these parameters was tested for an array of single quantum proton systems with widely varying character and geometry and was shown to provide accurate tunneling splittings and proton densities in all cases.²⁶ These prior benchmarking studies suggest that the overlap correction procedure and its associated parameters are both transferable and robust for the epc17-2 functional with a single quantum proton. As will be shown below, they are also transferable to systems with multiple quantum protons, with the possibility that reparameterization could be warranted for some types of systems. The NEO-MSDFT method with the overlap correction implemented was denoted as NEO-MSDFT' in the original paper, but for notational simplicity, we omit the prime for the remainder of this paper. The results without the corrected overlap are provided in the SI. Note that an alternative strategy would be to apply corrections to the epc17-2 functional or to develop new epc functionals specifically for NEO-MSDFT.

The NEO-MSDFT method captures both electron-electron and electron-proton static and dynamical correlation: static correlation is included through the expansion of each NEO-MSDFT state in terms of localized NEO-DFT diabatic states, and dynamical correlation is incorporated through the epc and conventional electronic exchange-correlation functionals. Static and dynamical correlation are not strictly separable, however, and therefore over-counting of these correlation effects could potentially be an issue with certain density functionals. The previous success of NEO-MSDFT in producing accurate tunneling splittings and proton densities for single quantum proton cases, ²⁶ as well as the results for multiple quantum proton cases below, indicates that such over-counting effects are not a significant issue in the NEO-MSDFT approach.

In NEO-MSDFT, two basis function centers are assigned for each transferring proton: one center is localized near the proton donor, and another center is localized near the proton acceptor. These centers are optimized variationally at the NEO-DFT level using the procedure described in the SI. The 2^N NEO-DFT diabatic states are obtained by choosing appropriately localized initial densities and performing NEO-DFT self-consistent field calculations, thereby producing the occupied coefficient matrices $\mathbf{C}_{i,o}^{e}$ and $\mathbf{C}_{i,o}^{p}$ for each diabatic state $|\tilde{\Psi}_{i}\rangle$. These

coefficients are used to compute the matrix elements of the Hamiltonian and overlap matrices of Eqs. (6) and (3), respectively. Then Eq. (2) is solved to obtain the adiabatic NEO-MSDFT states. As mentioned above, in practice fewer NEO-DFT diabatic states may be included in the expansion. We implemented the generalized NEO-MSDFT method in a development version of the Q-Chem 5.4 package.⁴⁷

We applied the generalized NEO-MSDFT approach to a series of geometries of the formic acid dimer and the cyano and amino-substituted formic acid dimer variants, as well as porphycene. We also investigated a protonated water chain composed of four water molecules to determine if NEO-MSDFT can properly capture the bilobal character of the excess proton and to demonstrate the capability of NEO-MSDFT to treat proton relays and other systems involving more than two transferring protons. For all NEO calculations, the B3LYP electronic exchange-correlation functional and the epc17-2 electron-proton correlation functional functional were used. All NEO calculations used the PB5-G protonic basis set for the quantum nuclei, with the exception that the PB4-D protonic basis set were used for the water chain. The aug-cc-pVDZ and aug-cc-pV5Z electronic basis sets were used for the classical and quantum nuclei, respectively, with the exception that the cc-pVDZ electronic basis was used for the classical nuclei of porphycene.

We benchmarked the NEO-MSDFT method by comparing the calculated tunneling splittings to those computed with the Fourier Grid Hamiltonian (FGH) method, 51 which is numerically exact for electronically adiabatic systems. We performed both two-dimensional (2D) FGH calculations, where each proton moves in one dimension along its proton transfer axis, and four-dimensional (4D) FGH calculations, where each proton moves on a 2D grid in the plane of the molecule. Here, the tunneling splitting, denoted as ΔE_{01} , is defined as the energy difference between the first vibrationally excited state and the ground vibrational state. As shown in the calculations below, the NEO-MSDFT method captures the symmetric ground state and antisymmetric first excited vibrational state characteristic of symmetric or nearly symmetric double-well systems. However, the NEO-MSDFT method does not provide meaningful higher vibrational states because the diabatic basis used here does not include bending modes. In

principle, the diabatic basis could be expanded to include such modes, but for most purposes the lowest two vibronic states are sufficient to describe hydrogen tunneling dynamics.

Our first generalized NEO-MSDFT calculations focus on the formic acid dimer and cyanoand amino-substituted variants. The procedure for obtaining symmetric or nearly symmetric geometries of these systems is discussed in the SI. The resulting geometries are shown in the insets of Figures 1B, 1D, and 1F. The 2D proton potential energy surfaces, as well as onedimensional slices, for the formic acid dimer, cyano-substituted dimer, and amino-substituted dimer at the equilibrium carbon-carbon distance of the formic acid dimer, which is 3.80 Å, are shown in Figure 1. The potentials were calculated by generating a two-dimensional grid for each structure, where each of the transferring protons moved in one dimension along its proton transfer axis connecting its donor and acceptor oxygen atoms. See the SI for more details about these calculations.

For each 2D potential energy surface in Figure 1, the two minima correspond to the two trans structures. In other words, one minimum corresponds to the top proton on its donor oxygen and the bottom proton on its acceptor oxygen, and the other minimum corresponds to the top proton on its acceptor oxygen and the bottom proton on its donor oxygen. When one proton is at the origin, the slice along the other proton coordinate is a double-well potential energy curve that is symmetric for the formic acid dimer and slightly asymmetric for the substituted formic acid dimers (black curves in Figures 1B, 1D, and 1F). When one proton is either at a negative or positive value, the double-well potential energy curve becomes significantly asymmetric (blue and red curves in Figures 1B, 1D, and 1F).

Seven different geometries were studied for each of the three formic acid dimer systems. For the unsubstituted formic acid dimer, the first geometry was the averaged equilibrium structure depicted in Figure 1B, three of the geometries were generated by moving the two rigid monomers of this structure closer together by increments of 0.02 Å, and another three were generated by moving the two rigid monomers of this structure further apart by increments of 0.02 Å. For the two substituted formic acid dimers, the seven geometries were generated in an analogous manner. Thus, each of the seven different geometries for each of the three formic acid dimer

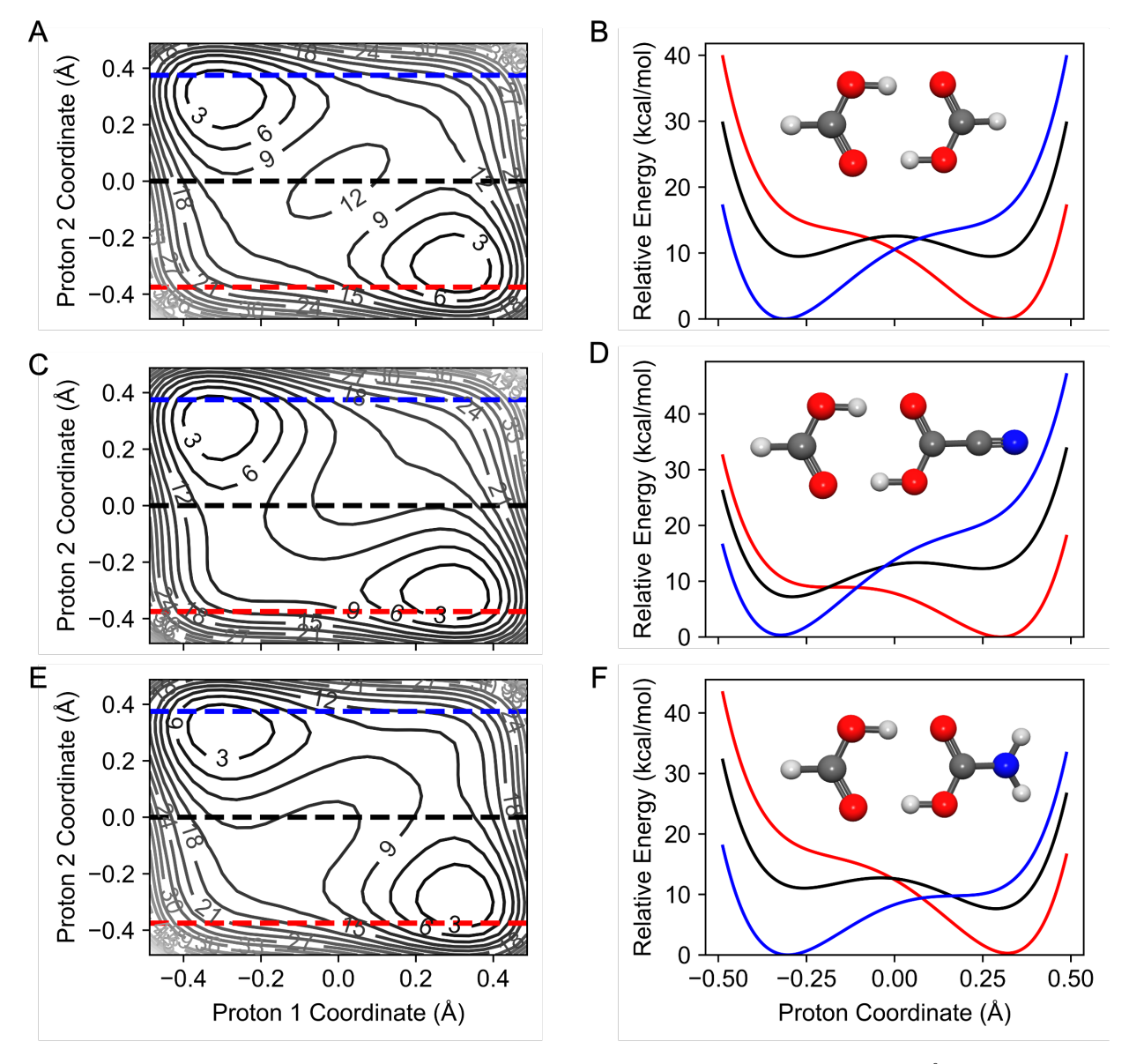


Figure 1. Potential energies computed at a carbon-carbon distance of 3.80 Å for (A, B) the formic acid dimer, (C, D) the cyano-substituted formic acid dimer, and (E, F) the amino-substituted formic acid dimer. The two-dimensional proton potential energy surfaces (A, C, E) are plotted as a function of the two proton coordinates, each corresponding to a one-dimensional grid spanning the associated oxygen-oxygen axis. The origin of each proton coordinate corresponds to the midpoint between the oxygen atoms, and the energies are computed relative to the minimum energy for each system. Relative energies in kcal/mol are provided on each contour line. The one-dimensional proton potential energy curves (B, D, F) correspond to slices of the two-dimensional surfaces along proton 1 coordinate with the proton 2 coordinate fixed to a position of -0.375 Å (red), 0 Å (black), and +0.375 Å (blue). The corresponding colored dashed lines of (A, C, E) indicate these one-dimensional slices on the two-dimensional potential energy surfaces.

systems has a different distance between its two carbon atoms, denoted as $R_{\rm CC}$. The tunneling splittings were computed with the 2D FGH method for all 21 geometries and with the 4D FGH method for 9 geometries (i.e., 3 per system). We found that the 4D FGH splittings were consistently $\sim 75\%$ of the 2D FGH splittings. Therefore, we used the 4D FGH splittings as the benchmark, scaling the splittings that were only computed with the 2D FGH method. All computed 2D and 4D FGH splittings are provided in the SI in Table S1.

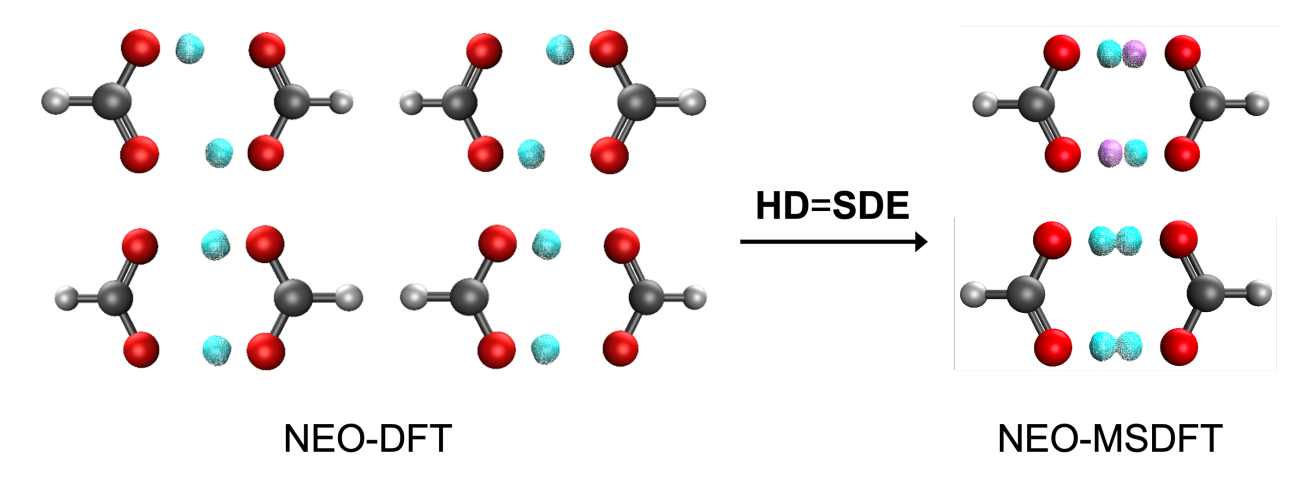


Figure 2. Visual representation of the generalized NEO-MSDFT procedure for the case of the unsubstituted formic acid dimer. Four possible NEO-DFT diabatic states (left) are linearly combined to produce the adiabatic NEO-MSDFT states, where only the ground and first excited vibronic states (right) are meaningful. In practice, only the *trans* NEO-DFT diabatic states (top left) were used to compute the tunneling splittings for these systems.

The four possible diabatic states for the formic acid dimer, as well as the adiabatic ground and excited NEO-MSDFT states, are shown in Figure 2. The tunneling splitting for each geometry was calculated with NEO-MSDFT using the two diabatic states corresponding to the trans positions of the transferring protons. The two diabatic states corresponding to the cis positions of the transferring protons were not included because they are much higher in energy, as indicated by the potential energy surfaces, which do not exhibit minima corresponding to cis structures (Figure 1). Calculations that include the cis diabatic states are discussed in the SI. A comparison of the NEO-MSDFT tunneling splittings and those calculated with the FGH reference method is provided in Figure 3 and Table 1. The tunneling splittings calculated with NEO-MSDFT are in good agreement with the benchmark FGH results for all $R_{\rm CC}$ tested for

all three dimer systems.

Table 1. Tunneling Splittings (in cm⁻¹) of the Three Formic Acid Dimer Systems at Varying Carbon-Carbon Distances, $R_{\rm CC}$, Calculated with FGH and NEO-MSDFT ^a

Substituent	$R_{\rm CC}$ (Å)	FGH	NEO-MSDFT
None	3.74	46.64	49.33
	3.76	23.36	27.29
	3.78	11.37	14.64
	3.80	5.16	7.48
	3.82	2.31	3.50
	3.84	0.99	1.36
	3.86	0.41	0.31
CN	3.74	68.23	50.90
	3.76	34.47	27.21
	3.78	16.75	14.41
	3.80	7.47	7.41
	3.82	3.32	3.45
	3.84	1.39	1.33
	3.86	0.56	0.30
NH_2	3.74	62.15	53.00
	3.76	31.40	28.84
	3.78	15.35	15.37
	3.80	6.94	8.05
	3.82	3.10	3.82
	3.84	1.31	1.53
	3.86	0.54	0.40

^a The substituent is only added to one monomer in the dimer. The NEO-MSDFT calculations include only the two *trans* states. The FGH results are 4D for all geometries where $R_{\rm CC}$ is 3.74, 3.80, and 3.86 Å, and scaled 2D for all other distances.

To further investigate the NEO-MSDFT results, we analyzed the proton densities. Figure 3 shows the ground state NEO-MSDFT proton densities for one of the protons along the line connecting the proton basis function centers for select dimer geometries. (Note that the two protons are equivalent in these systems.) All calculated proton densities exhibit their anticipated symmetry. The unsubstituted formic acid dimer system has a completely symmetric ground and first excited state proton density for all $R_{\rm CC}$, whereas the cyano and amino-substituted dimer structures have ground and first excited state proton densities with an asymmetry that can be explained by the electron-donating and electron-withdrawing effects of the substituents. The

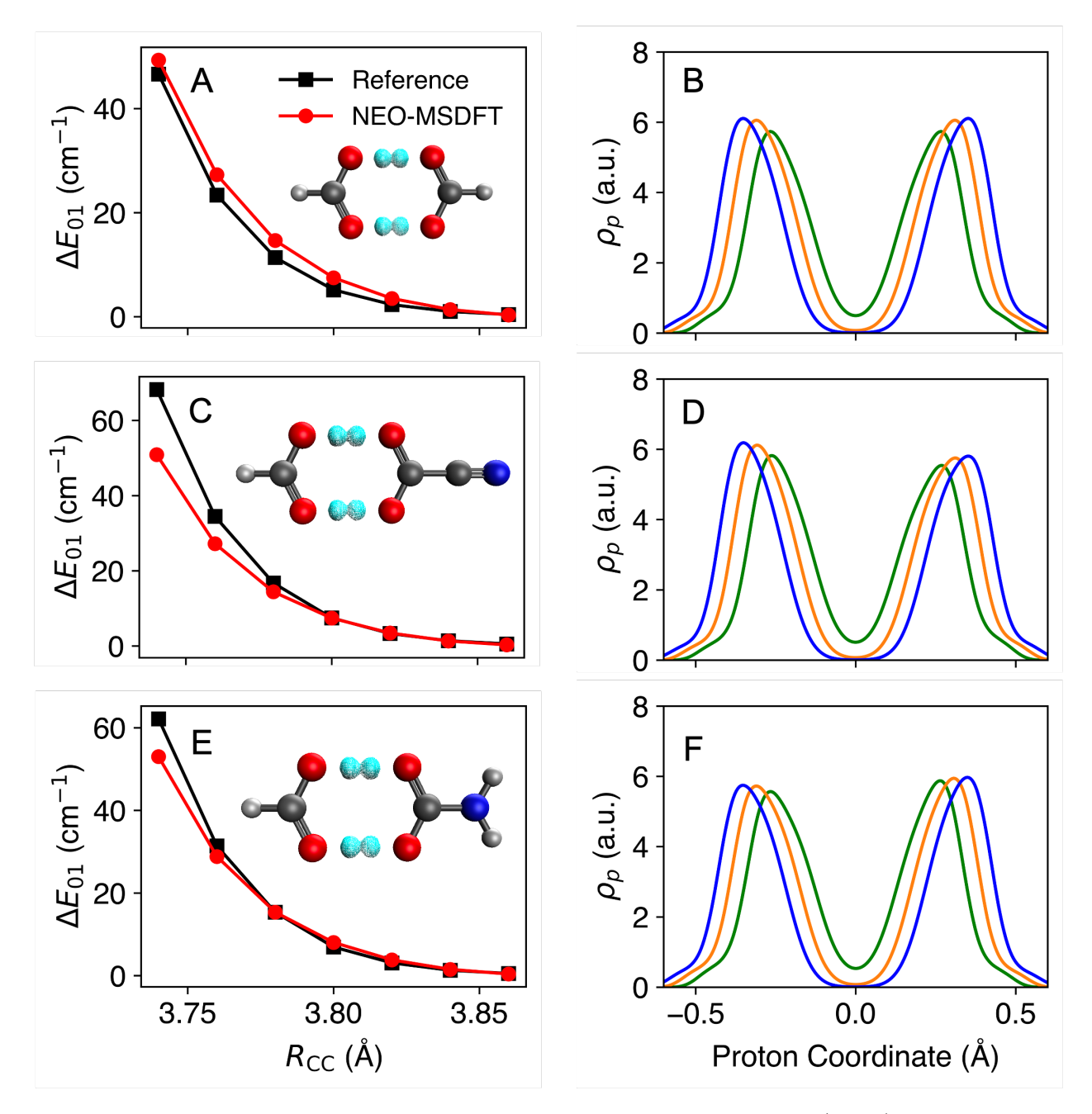


Figure 3. Tunneling splittings and ground state proton densities of (A, B) the formic acid dimer, (C, D) the cyano-substituted formic acid dimer, and (E, F) the amino-substituted formic acid dimer at varying $R_{\rm CC}$. The NEO-MSDFT calculations were performed with two diabatic states, and the reference results are 4D FGH or scaled 2D FGH calculations. The insets of (A, C, E) depict the ground state NEO-MSDFT proton densities in cyan. The tunneling splittings are also provided in Table 1. In (B, D, F), the proton densities are plotted along the line connecting the proton basis function centers for one of the protons with $R_{\rm CC} = 3.74$ Å (green), $R_{\rm CC} = 3.80$ Å (orange), and $R_{\rm CC} = 3.86$ Å (blue).

cyano group is electron withdrawing and the amino group is electron donating, corresponding to a larger proton density on the left and right sides, respectively (Figures 3C and 3E). All proton densities also exhibit their expected nodal character. The ground state densities do not exhibit any nodes, whereas the first exited state densities exhibit nodes at a proton coordinate of zero (Figure S1). This is directly analogous to the symmetric ground state and antisymmetric first excited state wavefunctions characteristic of double-well systems. All proton densities also followed the expected trend with increasing $R_{\rm CC}$, where the peaks of each density shift further away from each other as the rigid monomers move further apart.

We now turn our attention toward the larger porphycene system. Porphycene is distinct from the formic acid dimer in that the double proton transfer is mediated by the aromatic structure of the macrocycle. The structure of porphycene is shown in Figure 4, and the procedure for obtaining this geometry is discussed in the SI. The two-dimensional proton potential energy surfaces and one-dimensional slices for porphycene are shown in Figures 4A and 4B, respectively. In contrast to the formic acid dimer, these surfaces exhibit distinct minima at the *cis* geometries as well as the *trans* geometries. Thus, we included all four diabatic states in the NEO-MSDFT calculations. The resulting ground and first excited state proton vibrational wavefunctions and densities are shown in Figures 4C and Figure 4D, respectively. As observed for the formic acid dimer, the ground state wavefunction is symmetric, and the first excited state wavefunction is antisymmetric. Moreover, the ground state density has some amplitude in the classically forbidden region (i.e., at a proton coordinate of zero), whereas the first excited state has a node at this coordinate. The tunneling splitting for porphycene was found to be 37.63 cm⁻¹ and 44.84 cm⁻¹ using the (unscaled) 2D FGH method and the NEO-MSDFT method, respectively. This agreement is remarkable considering that the calculations did not involve any free parameters.

As a final application, we show that the generalized NEO-MSDFT procedure can capture the proton density associated with a proton relay system. A protonated water chain composed of four water molecules was optimized with conventional DFT for fixed O-O distances of 2.70 Å between neighboring oxygens while constraining the central proton to be equidistant from its two neighboring oxygen atoms. See the SI for further details about how this geometry was

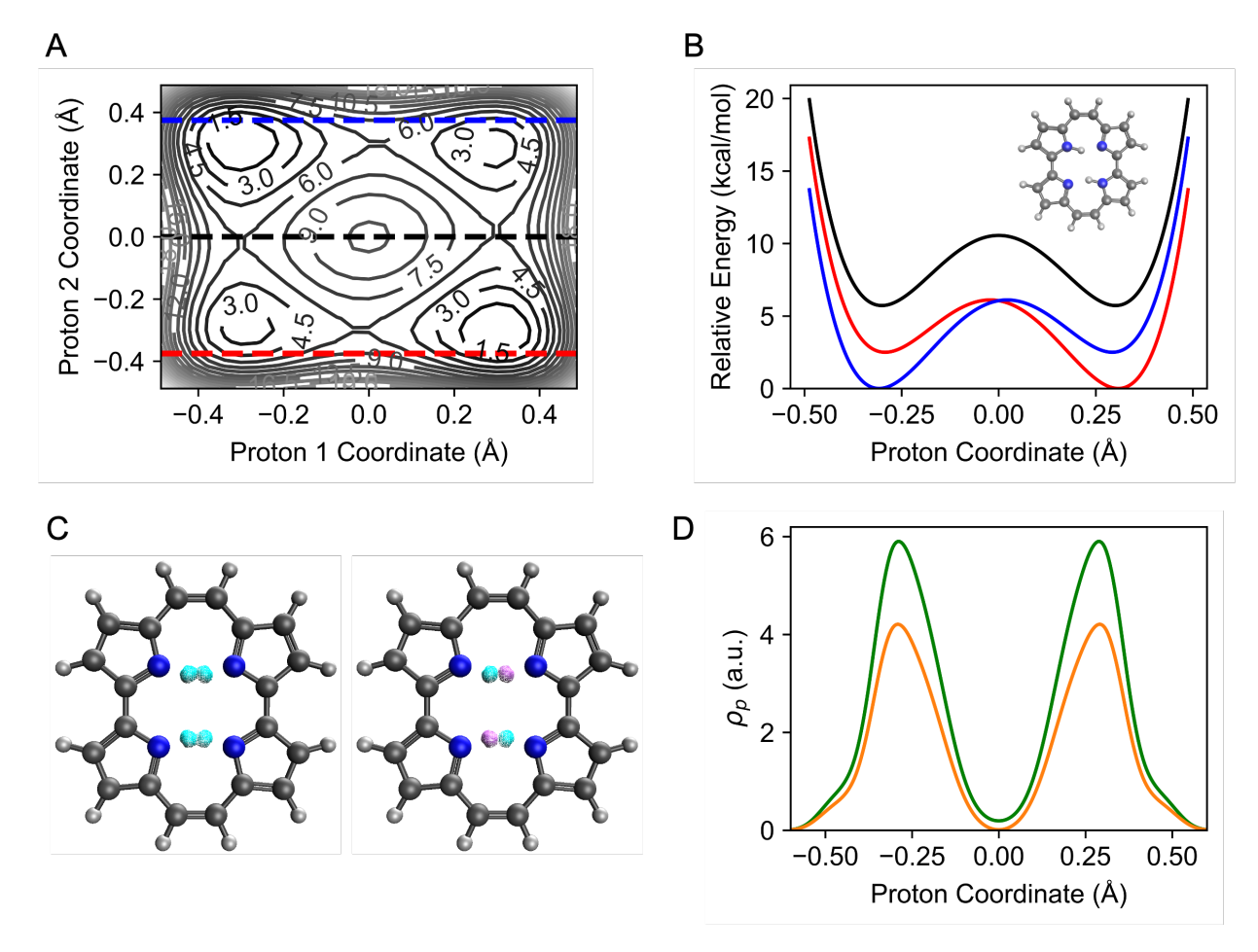


Figure 4. (A) Two-dimensional proton potential energy surface as a function of the two proton coordinates, each corresponding to a one-dimensional grid spanning the line connecting the proton positions optimized at the conventional DFT level for the two trans structures, with the origin at the midpoint between them. Relative energies in kcal/mol are provided on each contour line. (B) One-dimensional proton potential energy curves corresponding to slices of the two-dimensional surface along proton 1 coordinate with proton 2 coordinate fixed to a position of -0.375 Å (red), 0 Å (black), and +0.375 Å (blue). The corresponding colored dashed lines of (A) indicate these one-dimensional slices on the two-dimensional potential energy surface. (C) Ground state (left) and first excited state (right) NEO-MSDFT proton densities. To visualize the phase of the corresponding proton vibrational wavefunction, the positive and negative phases are shown in cyan and purple, respectively. (D) Ground state (green) and first excited state (orange) proton densities computed with NEO-MSDFT along one of the proton transfer coordinates.

generated. This water chain can be viewed as a snapshot during the Grotthuss mechanism of proton transport down the chain,⁵² where the proton is delocalized between the middle two oxygens in this snapshot. From the conventional Born-Oppenheimer perspective, each of the three transferring protons is moving in a double-well potential: the two outer transferring protons move in highly asymmetric double-well potentials, whereas the central transferring proton moves in a nearly symmetric double-well potential.

We performed an eight-state NEO-MSDFT calculation on this system with all nine protons quantized. Only the three transferring protons were represented by two basis function centers rather than a single basis function center. A description for how the basis function center positions were determined is provided in the SI. The eight possible diabatic states associated with the three transferring protons were included in the NEO-MSDFT calculation, producing the ground state proton density shown in Figure 5B. For comparison, a single-reference NEO-DFT calculation was performed using the same geometry and the same positions of the basis function centers, and its proton density is shown in Figure 5A.

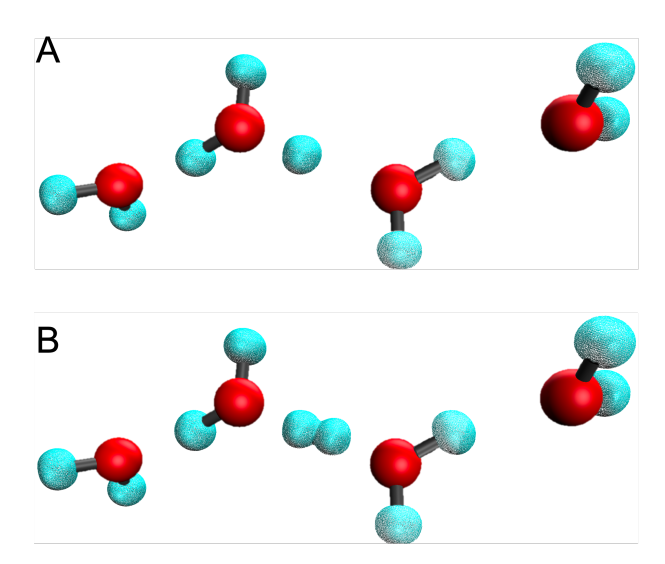


Figure 5. A protonated water chain composed of four water molecules, where all nine protons are quantized with the NEO approach. The ground state proton densities calculated using (A) NEO-DFT and (B) NEO-MSDFT are shown in cyan. Bonds are drawn between the localized quantum protons and the closest oxygen for visual clarity. NEO-MSDFT is able to capture the bilobal character of the central proton density, whereas NEO-DFT cannot capture this tunneling behavior.

The NEO-MSDFT method is able to capture the bilobal density of the central proton while

also predicting that the two outer transferring protons remain localized near their respective oxygen atoms. In contrast, the single-reference NEO-DFT calculation incorrectly predicts the central proton to be localized near one of its neighboring oxygen atoms. Thus, the NEO-MSDFT method is able to describe the tunneling character of the excess central proton while appropriately weighting all eight diabatic states such that the outer transferring protons remain localized.

This work presents a generalized NEO-MSDFT approach for treating systems with multiple quantum protons that are transferring and possibly tunneling. In this approach, NEO-DFT diabatic states, corresponding to each proton localized near its donor or acceptor, are linearly combined to produce NEO-MSDFT adiabatic states. The ground and first excited NEO-MSDFT vibronic states are able to capture the approximately symmetric and antisymmetric characteristics of proton wavefunctions for tunneling systems. This approach provides accurate tunneling splittings for the formic acid dimer, as well as the asymmetric cyano- and amino-substituted formic acid dimers, for a range of distances between the monomers. It also predicts a reasonably accurate tunneling splitting for porphycene. redThe application to a protonated water chain with nine quantum protons illustrates that NEO-MSDFT can describe a combination of localized and delocalized, bilobal proton densities within a single system. Note that the tunneling splittings computed herein are not directly comparable to experimentally measured splittings because they were computed at fixed geometries and do not include coupling to other vibrational modes of the molecule. The generalized NEO-MSDFT method can be combined with vibronic coupling theory⁵³ to include this coupling and with nonadiabatic dynamics methods to describe tunneling dynamics.³⁴

In addition to providing an accurate description of hydrogen tunneling, the NEO-MSDFT approach also allows smooth transitioning between localized NEO-DFT solutions while accurately describing proton delocalization and avoiding complications of local minima in orbital space. In other words, this approach can describe both asymmetric systems, in which the proton density is localized, and symmetric or nearly symmetric systems, in which the proton density is delocalized and possibly bilobal. When coupled to a hybrid quantum mechanical/molecular

mechanical approach,⁵⁴ the generalized NEO-MSDFT approach will enable quantum dynamics simulations of many types of multiple proton transfer processes, such as extended proton relay systems and complex mechanisms in enzymatic active sites.

Supporting Information

Details on calculating the NEO-MSDFT proton density; excited state proton densities of formic acid dimer systems; additional tunneling splitting results for formic acid dimer systems; details about procedures for geometry optimizations and determination of basis function center positions; computational details about FGH calculations; Cartesian coordinates of molecular geometries.

Acknowledgement

The authors thank Dr. Tao Li, Dr. Chris Malbon, Dr. Jonathan Fetherolf, Dr. Eno Paenurk, Dr. Alexander Soudackov, Mathew Chow, Millan Welman, and Rachel Stein for useful discussions. This work was supported by the National Science Foundation Grant No. CHE-1954348.

J. A. D. was also supported by the National Institutes of Health Grant 5T32GM008283.

References

- (1) Cha, Y.; Murray, C. J.; Klinman, J. P. Hydrogen Tunneling in Enzyme Reactions. *Science* 1989, 243, 1325–1330.
- (2) Hammes-Schiffer, S. Hydrogen Tunneling and Protein Motion in Enzyme Reactions. *Acc. Chem. Res.* **2006**, *39*, 93–100.
- (3) Richardson, J. O.; Pérez, C.; Lobsiger, S.; Reid, A. A.; Temelso, B.; Shields, G. C.; Kisiel, Z.; Wales, D. J.; Pate, B. H.; Althorpe, S. C. Concerted Hydrogen-Bond Breaking by Quantum Tunneling in the Water Hexamer Prism. *Science* **2016**, *351*, 1310–1313.

- (4) Habershon, S.; Manolopoulos, D. E.; Markland, T. E.; Miller, I., Thomas F. Ring-Polymer Molecular Dynamics: Quantum Effects in Chemical Dynamics from Classical Trajectories in an Extended Phase Space. Annu. Rev. Phys. Chem. 2013, 64, 387–413.
- (5) Litman, Y.; Richardson, J. O.; Kumagai, T.; Rossi, M. Elucidating the Nuclear Quantum Dynamics of Intramolecular Double Hydrogen Transfer in Porphycene. J. Am. Chem. Soc. 2019, 141, 2526–2534.
- (6) Vaillant, C. L.; Wales, D. J.; Althorpe, S. C. Tunneling Splittings in Water Clusters from Path Integral Molecular Dynamics. *J. Phys. Chem. Lett.* **2019**, *10*, 7300–7304.
- (7) Meyer, H. D.; Manthe, U.; Cederbaum, L. S. The Multi-Configurational Time-Dependent Hartree Approach. *Chem. Phys. Lett.* **1990**, *165*, 73–78.
- (8) Beck, M. H.; Jäckle, A.; Worth, G. A.; Meyer, H.-D. The Multiconfiguration Time-Dependent Hartree (MCTDH) Method: A Highly Efficient Algorithm for Propagating Wavepackets. *Phys. Rep.* **2000**, *324*, 1–105.
- (9) Hammer, T.; Coutinho-Neto, M. D.; Viel, A.; Manthe, U. Multiconfigurational Time-Dependent Hartree Calculations for Tunneling Splittings of Vibrational States: Theoretical Considerations and Application to Malonaldehyde. J. Chem. Phys. 2009, 131, 224109.
- (10) Webb, S. P.; Iordanov, T.; Hammes-Schiffer, S. Multiconfigurational Nuclear-Electronic Orbital Approach: Incorporation of Nuclear Quantum Effects in Electronic Structure Calculations. J. Chem. Phys. 2002, 117, 4106–4118.
- (11) Pavošević, F.; Culpitt, T.; Hammes-Schiffer, S. Multicomponent Quantum Chemistry: Integrating Electronic and Nuclear Quantum Effects via the Nuclear-Electronic Orbital Method. Chem. Rev. 2020, 120, 4222-4253.
- (12) Fabijan, P.; Culpitt, T.; Hammes-Schiffer, S. Multicomponent Coupled Cluster Singles and Doubles Theory within the Nuclear-Electronic Orbital Framework. J. Chem. Theory Comput. 2018, 15, 338–347.

- (13) Pavošević, F.; Rousseau, B. J. G.; Hammes-Schiffer, S. Multicomponent Orbital-Optimized Perturbation Theory Methods: Approaching Coupled Cluster Accuracy at Lower Cost. *J. Phys. Chem. Lett.* **2020**, *11*, 1578–1583.
- (14) Pak, M. V.; Chakraborty, A.; Hammes-Schiffer, S. Density Functional Theory Treatment of Electron Correlation in the Nuclear-Electronic Orbital Approach. J. Phys. Chem. A 2007, 111, 4522–4526.
- (15) Brorsen, K. R.; Yang, Y.; Hammes-Schiffer, S. Multicomponent Density Functional Theory: Impact of Nuclear Quantum Effects on Proton Affinities and Geometries. J. Phys. Chem. Lett. 2017, 8, 3488–3493.
- (16) Yang, Y.; Brorsen, K. R.; Culpitt, T.; Pak, M. V.; Hammes-Schiffer, S. Development of a Practical Multicomponent Density Functional for Electron-Proton Correlation to Produce Accurate Proton Densities. J. Chem. Phys. 2017, 147, 114113.
- (17) Yang, Y.; Culpitt, T.; Hammes-Schiffer, S. Multicomponent Time-Dependent Density Functional Theory: Proton and Electron Excitation Energies. J. Phys. Chem. Lett. 2018, 9, 1765–1770.
- (18) Zhao, L.; Tao, Z.; Pavošević, F.; Wildman, A.; Hammes-Schiffer, S.; Li, X. Real-Time Time-Dependent Nuclear-Electronic Orbital Approach: Dynamics beyond the Born-Oppenheimer Approximation. J. Phys. Chem. Lett. 2020, 11, 4052–4058.
- (19) Zhao, L.; Wildman, A.; Pavošević, F.; Tully, J. C.; Hammes-Schiffer, S.; Li, X. Excited State Intramolecular Proton Transfer with Nuclear-Electronic Orbital Ehrenfest Dynamics. J. Phys. Chem. Lett. 2021, 12, 3497–3502.
- (20) Tao, Z.; Yu, Q.; Roy, S.; Hammes-Schiffer, S. Direct Dynamics with Nuclear-Electronic Orbital Density Functional Theory. Acc. Chem. Res. 2021, 54, 4131–4141.
- (21) Tao, Z.; Yang, Y.; Hammes-Schiffer, S. Multicomponent Density Functional Theory: In-

- cluding the Density Gradient in the Electron-Proton Correlation Functional for Hydrogen and Deuterium. J. Chem. Phys. **2019**, 151, 124102.
- (22) Wang, Y.; Braams, B. J.; Bowman, J. M.; Carter, S.; Tew, D. P. Full-Dimensional Quantum Calculations of Ground-State Tunneling Splitting of Malonaldehyde Using an Accurate Ab Initio Potential Energy Surface. *J. Chem. Phys.* **2008**, *128*, 224314.
- (23) Schröder, M.; Gatti, F.; Meyer, H.-D. Theoretical studies of the Tunneling Splitting of Malonaldehyde Using the Multiconfiguration Time-Dependent Hartree Approach. J. Chem. Phys. 2011, 134–23, 234307.
- (24) Pak, M. V.; Hammes-Schiffer, S. Electron-Proton Correlation for Hydrogen Tunneling Systems. *Phys. Rev. Lett.* **2004**, *92*, 103002.
- (25) Pak, M. V.; Swalina, C.; Webb, S. P.; Hammes-Schiffer, S. Application of the Nuclear-Electronic Orbital Method to Hydrogen Transfer Systems: Multiple Centers and Multi-configurational Wavefunctions. *Chem. Phys.* **2004**, *304*, 227–236.
- (26) Yu, Q.; Hammes-Schiffer, S. Nuclear-Electronic Orbital Multistate Density Functional Theory. J. Phys. Chem. Lett. **2020**, 11, 10106–10113.
- (27) Mo, Y.; Bao, P.; Gao, J. Energy Decomposition Analysis Based on a Block-Localized Wavefunction and Multistate Density Functional Theory. *Phys. Chem. Chem. Phys.* **2011**, 13, 6760–6775.
- (28) Gao, J.; Grofe, A.; Ren, H.; Bao, P. Beyond Kohn–Sham Approximation: Hybrid Multistate Wave Function and Density Functional Theory. *J. Phys. Chem. Lett.* **2016**, *7*, 5143–5149.
- (29) Grofe, A.; Qu, Z.; Truhlar, D. G.; Li, H.; Gao, J. Diabatic-At-Construction (DAC) Method for Diabatic and Adiabatic Ground and Excited States Based on Multistate Density Functional Theory. J. Chem. Theory Comput. 2017, 13, 1176–1187.

- (30) Lu, Y.; Gao, J. Multistate Density Functional Theory of Excited States. *J. Phys. Chem. Lett.* **2022**, 7762–7769.
- (31) Skone, J. H.; Pak, M. V.; Hammes-Schiffer, S. Nuclear-Electronic Orbital Nonorthogonal Configuration Interaction Approach. *J. Chem. Phys.* **2005**, *123*, 134108.
- (32) Thom, A. J. W.; Head-Gordon, M. Hartree–Fock Solutions as a Quasidiabatic Basis for Nonorthogonal Configuration Interaction. *J. Chem. Phys.* **2009**, *131*, 124113.
- (33) Yu, Q.; Schneider, P. E.; Hammes-Schiffer, S. Analytical Gradients for Nuclear-Electronic Orbital Multistate Density Functional Theory: Geometry Optimizations and Reaction Paths. J. Chem. Phys. 2022, 156, 114115.
- (34) Yu, Q.; Roy, S.; Hammes-Schiffer, S. Nonadiabatic Dynamics of Hydrogen Tunneling with Nuclear-Electronic Orbital Multistate Density Functional Theory. *J. Chem. Theory Comput.* **2022**, *18*, 7132–7141.
- (35) Wilson, A. D.; Newell, R. H.; McNevin, M. J.; Muckerman, J. T.; DuBois, M. R.; DuBois, D. L. Hydrogen Oxidation and Production Using Nickel-Based Molecular Catalysts with Positioned Proton Relays. J. Am. Chem. Soc. 2006, 128, 358–366.
- (36) Bediako, D. K.; Solis, B. H.; Dogutan, D. K.; Roubelakis, M. M.; Maher, A. G.; Lee, C. H.; Chambers, M. B.; Hammes-Schiffer, S.; Nocera, D. G. Role of pendant Proton Relays and Proton-Coupled Electron Transfer on the Hydrogen Evolution Reaction by Nickel Hangman Porphyrins. Proc. Natl. Acad. Sci. 2014, 111, 15001–15006.
- (37) Drukker, K.; Hammes-Schiffer, S. An Analytical Derivation of MC-SCF Vibrational Wave Functions for the Quantum Dynamical Simulation of Multiple Proton Transfer Reactions: Initial Application to Protonated Water Chains. J. Chem. Phys. 1997, 107, 363–374.
- (38) Cukier, R. I. A Molecular Dynamics Study of Water Chain Formation in the Proton-Conducting K Channel of Cytochrome C Oxidase. *Biochim. Biophys. Acta.* **2005**, *1706*, 134–146.

- (39) Freier, E.; Wolf, S.; Gerwert, K. Proton Transfer via a Transient Linear Water-Molecule Chain in a Membrane Protein. *Proceedings of the National Academy of Sciences* **2011**, 108, 11435–11439.
- (40) Hsiao, Y.-W.; Gotze, J. P.; Thiel, W. The Central Role of Gln63 for the Hydrogen Bonding Network and UV-visible Spectrum of the AppA BLUF Domain. J. Phys. Chem. B. 2012, 116, 8064–8073.
- (41) Mil'nikov, G. V.; Kühn, O.; Nakamura, H. Ground-State and Vibrationally Assisted Tunneling in the Formic Acid Dimer. *J. Chem. Phys.* **2005**, *123*, 074308.
- (42) Barnes, G. L.; Squires, S. M.; Sibert, E. L. Symmetric Double Proton Tunneling in Formic Acid Dimer: A Diabatic Basis Approach. J. Phys. Chem. B 2008, 112, 595–603.
- (43) Jain, A.; Sibert, I., Edwin L. Tunneling Splittings in Formic Acid Dimer: An Adiabatic Approximation to the Herring Formula. *J. Chem. Phys.* **2015**, *142*, 084115.
- (44) Qu, C.; Bowman, J. An Ab Initio Potential Energy Surface for the Formic Acid Dimer: Zero-Point Energy, Selected Anharmonic Fundamental Energies, and Ground-State Tunneling Splitting Calculated in Relaxed 1–4-Mode Subspaces. *Phys. Chem. Chem. Phys.* 2016, 18, 24835–24840.
- (45) Richardson, J. O. Full- and Reduced-Dimensionality Instanton Calculations of the Tunnelling Splitting in the Formic Acid Dimer. *Phys. Chem. Chem. Phys.* **2017**, *19*, 966–970.
- (46) Cembran, A.; Song, L.; Mo, Y.; Gao, J. Block-Localized Density Functional Theory (BLDFT), Diabatic Coupling, and Their Use in Valence Bond Theory for Representing Reactive Potential Energy Surfaces. J. Chem. Theory Comput. 2009, 5, 2702–2716.
- (47) Epifanovsky, E. et al. Software for the Frontiers of Quantum Chemistry: An Overview of Developments in the Q-Chem 5 package. *J. Chem. Phys.* **2021**, *155*, 084801.
- (48) Lee, C.; Yang, W.; Parr, R. G. Development of the Colle-Salvetti Correlation-energy Formula into a Functional of the Electron Density. *Phys. Rev. B.* **1988**, *37*, 785.

- (49) Yu, Q.; Pavošević, F.; Hammes-Schiffer, S. Development of Nuclear Basis Sets for Multicomponent Quantum Chemistry Methods. *J. Chem. Phys.* **2020**, *152*, 244123.
- (50) Dunning, J., T. H. Gaussian Basis Sets for Use in Correlated Molecular Calculations: 1. The Atoms Boron through Neon and Hydrogen. J. Chem. Phys. 1989, 90, 1007–1023.
- (51) Webb, S. P.; Hammes-Schiffer, S. Fourier Grid Hamiltonian Multiconfigurational Self-Consistent-Field: A Method to Calculate Multidimensional Hydrogen Vibrational Wavefunctions. J. Chem. Phys. 2000, 113, 5214–5227.
- (52) Agmon, N. The Grotthuss Mechanism. Chem. Phys. Lett. 1995, 244, 456–462.
- (53) Hazra, A.; Skone, J. H.; Hammes-Schiffer, S. Combining the Nuclear-electronic Orbital Approach with Vibronic Coupling Theory: Calculation of the Tunneling Splitting for Malonaldehyde. J. Chem. Phys. 2009, 130, 054108.
- (54) Chow, M.; Lambros, E.; Li, X.; Hammes-Schiffer, S. Nuclear-Electronic Orbital QM/MM Approach: Geometry Optimizations and Molecular Dynamics. J. Chem. Theory Comput. DOI: 10.1021/acs.jctc.3c00361.